Precision Engineering 86 (2024) 265–275

Contents lists available at ScienceDirect

Precision Engineering

journal homepage: www.elsevier.com/locate/precision

Prediction of crack initiation in single-crystal sapphire during ultra-precision machining using MD simulation-based slip/fracture activation model

Suk Bum Kwon [a], Aditya Nagaraj [a], Dae Nyoung Kim [a], Dalei Xi [b], Yiyang Du [b], Woo Kyun Kim [b], Sangkee Min [a,*]

[a] Department of Mechanical Engineering, University of Wisconsin-Madison, Madison, 53706, Wisconsin, USA
[b] Department of Mechanical and Materials Engineering, University of Cincinnati, Cincinnati, 45221, Ohio, USA

ARTICLE INFO

Keywords:
Ductile-to-brittle transition
Molecular dynamics
Single-crystal sapphire
Slip/fracture activation model
Ultra-precision machining

ABSTRACT

In this paper, material deformation during ultra-precision machining (UPM) on the C-, R-, and A-planes of sapphire was investigated using the slip/fracture activation model where the likelihood of activation of individual plastic deformation and fracture systems on different crystallographic planes was calculated. The stress data obtained from molecular dynamics (MD) simulations were utilized, and the slip/fracture activation model was developed by incorporating the principal stresses in calculating the plastic deformation and fracture cleavage parameters. The analysis methodology was applied to study material deformation along various cutting orientations in sapphire. The stress field at crack initiation during UPM on C-, R-, and A-planes of sapphire was calculated using molecular dynamics (MD) simulations. An equation describing the relationship between crack initiation and its triggering parameters was formulated considering the systems' plastic deformation and cleavage fractures. The model can qualitatively predict the crack initiations for various cutting orientations. The proposed model was verified through ultra-precision orthogonal plunge cut experiments along the same cutting orientations as in the MD simulations.

1. Introduction

Various computer simulation techniques such as molecular dynamics (MD), smooth particle hydrodynamics (SPH), and quasi-continuum (QC) simulations have proved to be useful tools to understand deformations at the atomic level as the movement of individual atoms, dislocation motions, fracture initiation, and interaction between different deformations mechanisms can be visualized temporally [1]. In this regard, Matsunaga et al. studied the crack propagation mechanism in magnesium oxide ceramics and compared the MD simulations with in-situ TEM observations. The researchers observed atomic steps on the (010) plane along the cleaved surfaces due to dislocation nucleation in the vicinity of the crack tip which points to the interplay between plastic deformation and fracture [2]. Sun et al. studied the evolution of dislocation loops in single crystal 3C–SiC during nanoindentation using MD simulations. In this research, interactions between edge and screw dislocations and formation of prismatic loops were studied [3]. In the study by Bitzek et al. the interaction between dislocations and mode I cracks in single crystal nickel were studied. Depending on the orientation of the dislocation line with respect to the crack front, either a stimulated emission of dislocations, cross slip of the dislocation to a plane with a higher driving force, or no interaction between the crack and dislocation was observed. These interactions were attributed to changes in the local microstructure around a crack, thus controlling the ductile vs. brittle behavior [4]. A similar response was observed in the case of a brittle material – GaAs and a dependency on temperature was reported [5].

Specifically concerning ultra-precision machining, particularly of single crystal materials, material deformation is governed by the stress field in the tool-workpiece interface which is responsible for the activation of various slip/twinning/fracture systems. Although this is known, it is hard to exactly determine the stress field in the machining process due to complexities arising from the tool geometry, lateral movement of the tool in the workpiece, and interactions between the tool and workpiece material. Hence, simulation techniques such as FEM, MD simulations, and other methods provide valuable information in this regard. Although methodologies like FEM simulations allow for

* Corresponding author.
E-mail address: sangkee.min@wisc.edu (S. Min).

https://doi.org/10.1016/j.precisioneng.2023.12.007
Received 22 August 2023; Received in revised form 30 October 2023; Accepted 19 December 2023
Available online 24 December 2023

simulations at similar spatial and temporal scales to the experiments, the main issue in obtaining an accurate value of the stress field lies in the lack of a crystal plasticity material model for single crystal ceramics such as sapphire and the difficulties in accounting for fracture as well as plasticity in the same model. MD simulations don't have this limitation as they directly model material deformation based on atomic bonding. Many researchers have used MD simulations to gain insight into material deformation through indenter scratch and orthogonal cutting simulations. During MD simulations of nano scratching on single crystalline copper and iron using a pyramidal indenter, researchers observed a strong dependence of the pile-up height, groove depth, and scratching forces on the scratching direction due to activation of different plastic deformation mechanisms [6,7]. Pei et al. studied the influence of rake angle and tool edge radius on chip formation and elastic recovery during UPM of single crystalline copper. It was reported that a small edge radius and positive rake angle favored chip formation in the ductile material whereas a large edge radius or negative rake angle promoted plowing, as positive rake angles reduced the normal force to cutting force ratio [8]. Focusing on hard and brittle ceramics, many researchers have investigated the influence of different process parameters on the deformation behavior in materials such as silicon, silicon carbide, and sapphire [9,10]. Through MD simulations of UPM of silicon, Cai et al. observed that the compressive stress magnitude in the cutting zone decreases as the depth of cut is increased and is attributed as one of the reasons for the ductile to brittle transition [11]. In addition to deformation through slip activation and crack initiation, Goel et al. observed amorphization close to the surface and along grain boundaries during diamond cutting of single and polycrystalline silicon through MD simulations. Further analysis of atomic coordination numbers in the cutting region indicated high-pressure phase transformation [12].

Investigating the literature on sapphire, researchers have used MD simulations to mainly understand the effect of crystal anisotropy on deformation mechanisms, cutting forces, and subsurface damage during nano-scratching/indentation and orthogonal cutting on different planes of sapphire. Through nanoindentation on C-plane of sapphire, Lin et al. explained the activation of prismatic slips and influence of basal dislocations on phase transformation beneath the indenter [13]. Kim et al. investigated the atomic displacements and configuration in basal slip and rhombohedral twinning resulting from nanoindentation and scratching [14]. Wunderlich investigated the fracture toughness for four different crack orientations in sapphire using MD simulations [15].

From the surveyed literature, it is evident that an understanding of deformation mechanism activation and their interactions, based on three-dimensional stress state around the cutting tool is lacking. The current work aims to address this gap by using the stress state to calculate the tendency of activation of different deformation mechanisms. It is known that limitations in terms of the size and timescales of MD simulations exist when compared to experiments leading to simulations running at much higher strain rates. However, in this study, precedence was given to the effect that material properties would have on the stress field over the effect of strain rate.

In our previous research [16], the investigation of material deformation during UPM on the C-plane of sapphire utilized the slip/fracture activation model, which calculates the likelihood of activation of plastic deformation and fracture systems on different crystallographic planes. The previous analysis relied on stress data obtained from MD simulations, specifically focusing on the first principal stress to identify the crack initiation mechanism. In this paper, the authors have extended the slip/fracture activation model from the previous study by incorporating the second and third principal stresses in the calculation of plastic deformation and fracture cleavage parameters. The developed analysis methodology was applied to examine material deformation along various cutting orientations in sapphire using MD simulations. The analysis methodology was verified by performing ultra-precision orthogonal plunge cut experiments using the same cutting orientations as the MD simulations. In addition to this, by formulating a crack prediction model, the relationship between crack initiation and its triggering parameters was described. The proposed model provided a qualitative prediction of crack initiations for different cutting orientations.

2. Materials and methods

2.1. Crystal structure of sapphire and cutting orientations

Sapphire, belonging to the ditrigonal scalenohedral crystal class and space group 167 with R $\bar{3}$ c symmetry, exhibits a crystal structure composed of a hexagonal unit cell [17] and four functional crystallographic planes (A, C, M, and R). In this study, an orthogonal plunge cut was performed along 6 different cutting orientations on the C-, R-, and A-planes of the sapphire, considering two cutting orientations for each crystal plane as shown in Fig. 1 (*A*60°, *A*120°, *C*180°, *C*270°, *R*90°, and *R*180°). The angle θ_{cut} represents the deviation from 0° in the cutting direction, where 0° corresponds to [11 $\bar{2}$ 0] for C- and R-planes, and [0001] for A-plane. The cutting orientations are indicated by abbreviations of the respective planes and the value of θ_{cut}.

2.2. Molecular dynamics (MD) simulations

In this study, the interactions between the aluminum and oxygen atoms in sapphire were defined by the Vashishta potential [18] while the interactions between the indenter and substrate atoms were modeled through the Lennard-Jones potential [10,14].

The simulation model consisted of a rectangular sapphire substrate with approximate dimensions of 1500 Å × 30 Å x 1000 Å in the x, y, and z directions, respectively with a total of 4,500,000 atoms, Fig. 2. Periodic boundary condition (PBC) was applied in the y direction. The outermost layers of atoms on the bottom and one side were fixed to prevent any rigid body translations. A Langevin thermostat region was assigned adjacent to the fixed layer to absorb any excess heat generated from the deformation. The Newtonian region was assigned to the region above the thermostat region. The deformation takes place in this region. The tool was modeled as a rigid body having a diamond cubic structure consisting of about 68,500 atoms with an edge radius of 60 Å and a rake angle of −10°. Orthogonal cutting on the C-, R-, and A-planes of sapphire was conducted using LAMMPS (Large-scale Atomistic/Molecular Massively Parallel Simulator) software [19]. The cutting simulations were conducted along the 6 directions previously mentioned at a constant cutting depth of 400 Å and cutting speed of 100 m/s.

2.3. Experimental setup

Fig. 3 illustrates the experimental setup and provides a schematic view of the cutting process. For the experiment, a 5-axis ultra-precision CNC machine (ROBONANO α-0*i*B, FANUC Corp., Japan) with a command resolution of 1 nm in the 3 linear axes and 1 micro-degree in the 2 rotary axes was employed. The cutting tool (A.L.M.T. Corp., Japan) utilized was a binder-less nano-polycrystalline diamond tool with a 0.5 mm nose radius and 500 nm edge radius. The cutting parameters consisted of a cutting speed of 5 mm/min, a cutting slope of 1/500, and a rake angle of 0°. To ensure repeatability, the experiment was conducted three times. The substrate was mounted on a piezoelectric dynamometer (Type 911AA1, Kistler Instrument Corp., Switzerland) connected to a charge amplifier (Type 5080A with low pass filter, Kistler Instrument Corp., Switzerland), enabling real-time force measurement during the machining process. The measured force values were used to calculate the plastic deformation and cleavage fracture parameters for the experimental results [20]. The flatness of the workpiece was adjusted using a tilt stage and surface probe, while an optical microscope (SH140CCD-2R, Shodensha Inc., Japan) was used to establish the tool-work contact.

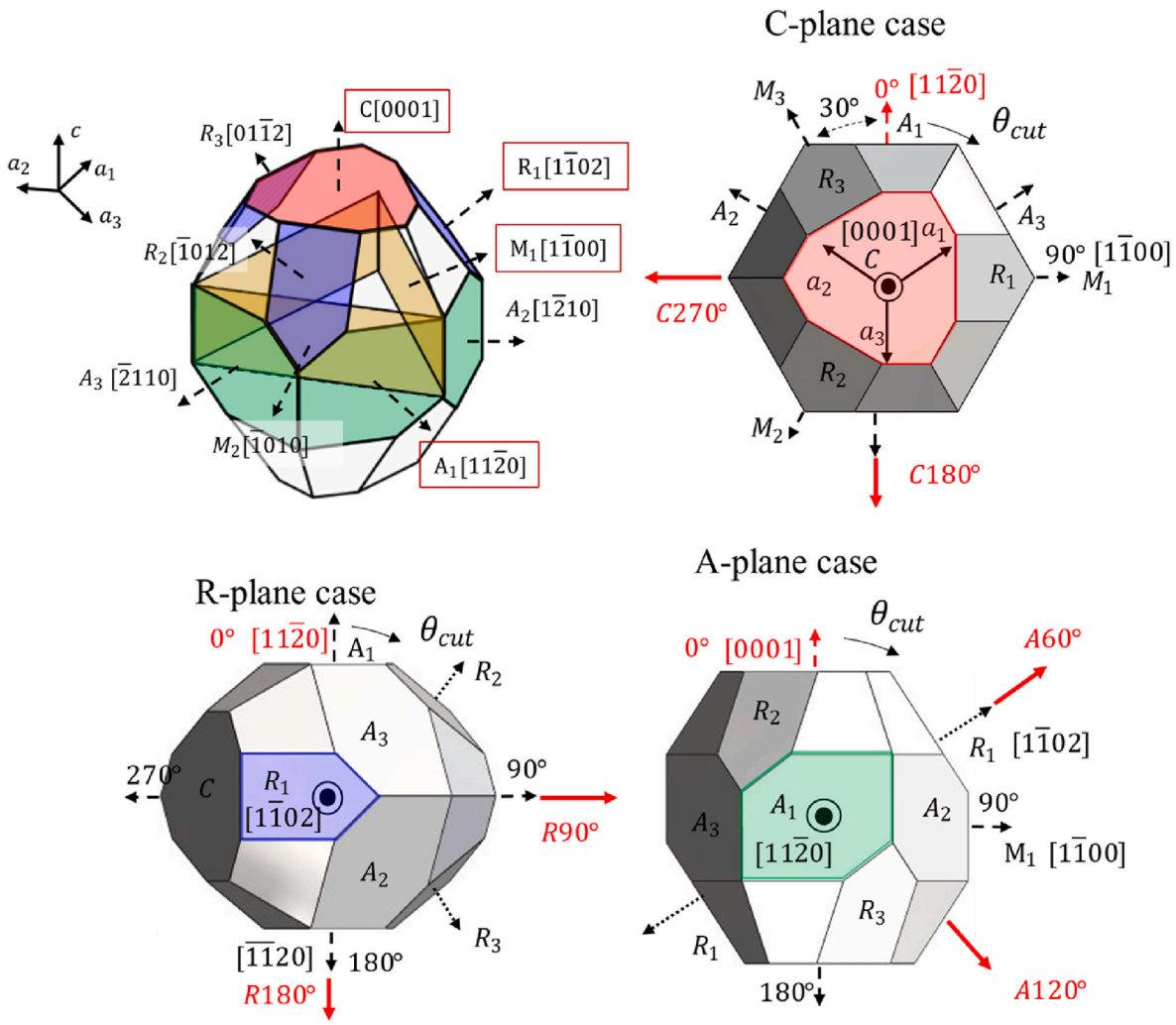

Fig. 1. Schematic view of crystallographic planes of sapphire and indication of cutting direction.

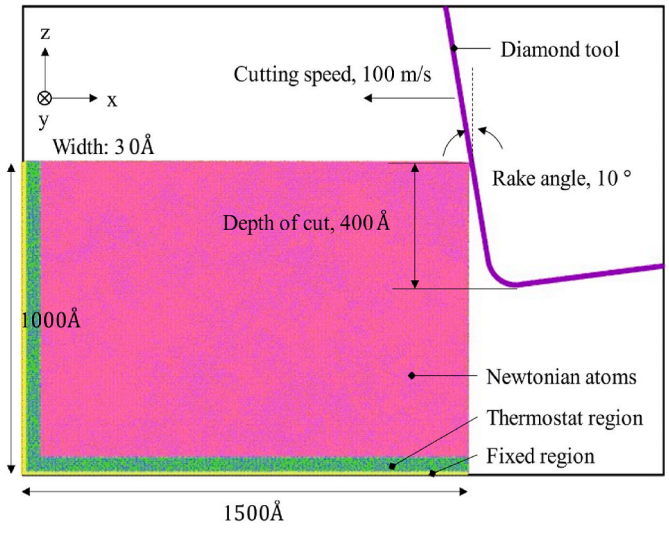

Fig. 2. Setup of molecular dynamics simulation of orthogonal cutting of sapphire.

2.4. Triaxial stress-based slip/fracture activation model

The material removal behavior in terms of crystallographic orientation was studied by calculating deformation activation parameters [16]. The previous model used only the first principal stress for calculating the activation parameters. In this paper, the model was extended by incorporating the second and third principal stresses in the calculation of the plastic deformation and fracture cleavage parameters. When Cauchy stress of a material point is given, the plastic deformation and cleavage fracture parameters can be calculated while accounting for the principal stresses using the following equations.

$$P_i^k = \left[\sum_{n=1}^{3} \hat{\sigma}_n^k \cos\left(\theta_{n,i}^k\right)\cos\left(\lambda_{n,i}^k\right)\right]\left[\min_i\left(\tau_{CRSS,i}\right) \Big/ \tau_{CRSS,i}\right] \quad (1)$$

$$F_j^k = \left[\sum_{n=1}^{3} \hat{\sigma}_n^k \cos^2\left(\varphi_{n,j}^k\right)\right]\left[\min_j\left(K_{CI,j}\right) \Big/ K_{CI,j}\right] \quad (2)$$

where P_i^k is the plastic deformation parameter of i^{th} slip/twinning system at the k^{th} material point, $\hat{\sigma}_n^k$ is the normalized n^{th} principal stress at the k^{th} material point, which equals to $\sigma_n^k \bullet \left(\sum_i^3 \sigma_i^k\right)^{-1}$. $\theta_{n,i}^k$ is the angle between $\hat{\sigma}_n^k$ and plane normal direction of the i^{th} slip/twinning system at the k^{th} material point, $\lambda_{n,i}^k$ is the angle between $\hat{\sigma}_n^k$ and slip/twinning direction of the i^{th} slip/twinning system at the k^{th} material point, Fig. 4

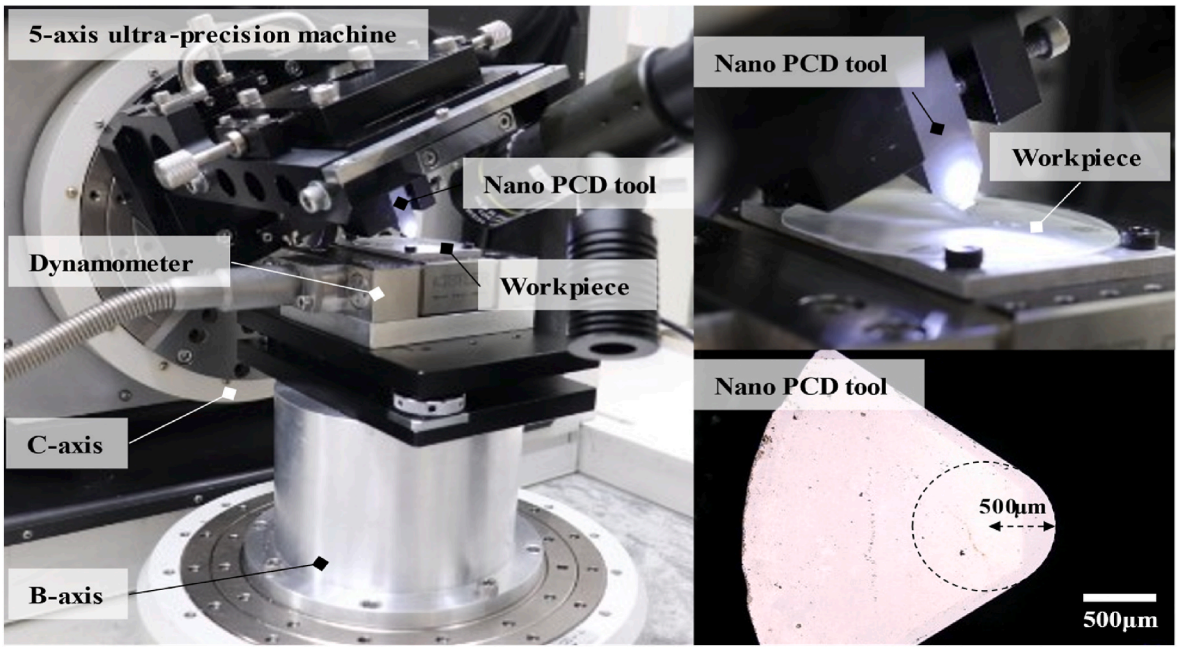

Fig. 3. Experimental setup and optical microscope image of rake face of cutting tool.

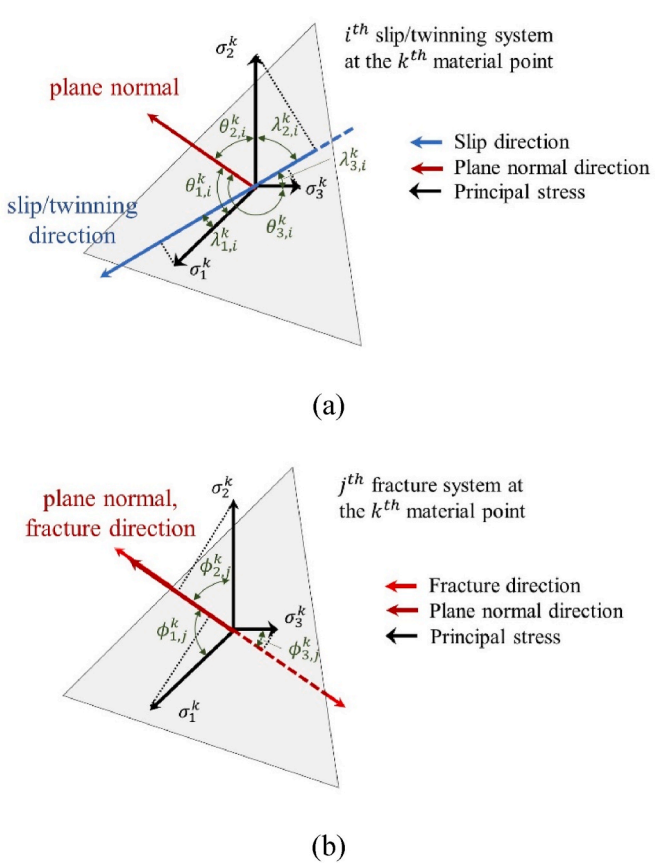

Fig. 4. Calculation of (a) plastic deformation parameter and (b) cleavage fracture parameter based on slip/fracture activation model.

(a). $\min_i(\tau_{CRSS,i})$ is the minimum critical resolved shear stress among all the possible slip/twinning systems, and $\tau_{CRSS,i}$ is the critical resolved shear stress of i^{th} slip/twinning system. F_j^k is the cleavage fracture parameter of the j^{th} fracture system at the k^{th} material point, $\varphi_{n,j}^k$ is the angle between $\hat{\sigma}_n^k$ and plane normal direction of the j^{th} fracture system at the k^{th} material point, Fig. 4 (b). $\min_j(K_{CI,j})$ is the minimum mode I critical stress intensity factor among all the fracture systems, and $K_{CI,j}$ is the mode I critical stress intensity factor of the j^{th} fracture system. The values of critical resolved shear stress and critical stress intensity factor are indicated in Tables 1 and 2, respectively.

3. Result and discussion

3.1. Deformation activation predicted using plastic deformation parameter

The stress values obtained from MD simulations can be considered as comparable to experimental results, as well as critical resolved shear stress and critical stress intensity factor values which are material properties. Considering that the calculation of plastic deformation and cleavage fracture parameters rely on these values, the stress values from MD simulations were used to calculate the plastic deformation and cleavage fracture parameters to better understand material removal behavior during UPM and were compared with experimental results. The activated deformation system was identified by plotting the shear strain using OVITO, a software enabling post-processing or 3-dimensional visualization of atomic data obtained from MD or Monte Carlo simulations [23], and measuring the angle made by the plane of deformed atoms with the workpiece surface. The shear strains were plotted at 60 ps, where one or two plastic deformations were clearly and distinguishably observed in all six cutting orientations. To confirm the effectiveness of the slip/fracture activation model, results from the

Table 1
Slip/twinning systems of single-crystal sapphire [21].

Slip/twinning system	Miller-Bravais Indices	Critical Resolved Shear Stress [MPa]
Basal twinning (C-)	(0001) < $\bar{1}$ 010>	2.2255
Basal slip (C-)	(0001) <11 $\bar{2}$ 0>	2.2255
Prismatic slip (A-)	{11 $\bar{2}$ 0} <$\bar{1}$ 100>	1.6487
Rhombohedral twinning (R-)	{1 $\bar{1}$ 02} <10$\bar{1}$ 1>	0.4066

Table 2
Fracture systems of single-crystal sapphire [22].

Fracture system	Miller-Bravais indices	Critical stress intensity factor $\frac{1}{[MPa \cdot m^{\frac{1}{2}}]}$
Basal fracture (C-)	(0001)	4.54
Prismatic fracture (M −)	{10 $\bar{1}$ 0}	3.14
Rhombohedral fracture (R-)	{1$\bar{1}$ 02}	2.38
Prismatic fracture (A-)	{11 $\bar{2}$ 0}	2.43

model were compared with the shear strain plots. A specific target area with a radius of 50 Å was defined within the region where deformation was observed and the average value of the plastic deformation parameters for material points within this designated area was calculated.

Fig. 5 (a) displays the shear strain plot at t_{cut} = 60 ps for the C270°○ cutting orientation and the activated deformation mechanisms have been identified. A schematic view of the crystal structure is included to aid in comprehension. The plot reveals the activation of R_{2tw} and R_{3tw} twinning systems in the depth direction, as well as the activation of the R_{1tw} twinning system towards the surface. The labels were set according to the type of plastically deformed or cleaved plane and its activation. R, C, A, and M represent the rhombohedral, basal, 1st prismatic, and 2nd prismatic planes, while *tw* and *sl* represent activation of twinning and slip systems, respectively.

Fig. 5 (b) temporally shows the average values of the plastic deformation parameters in the designated target area. The results demonstrate a significant likelihood of R_{1tw}, R_{2tw}, and R_{3tw} twinning systems, consistent with the observed results. This finding indicates that the calculated plastic deformation parameters accurately predicted the dominant deformation mechanism in the MD simulation of C270°cutting orientation.

Table 3 presents a summary of the deformation systems observed in the shear strain plots in OVITO and the predicted deformation systems

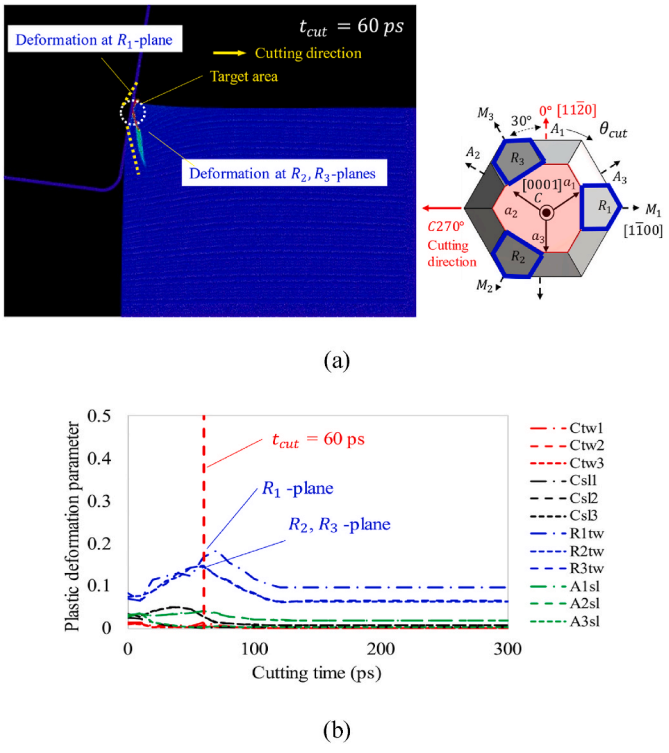

Fig. 5. (a) Deformation activations observed by MD simulation and (b) calculated plastic deformation parameters in the target area for C270° cutting orientation.

Table 3
Summary of observed/predicted plastic deformation systems.

	System	1st	2nd	3rd	4th	5th
*A*60°	Observed	A_{2sl}	A_{3sl}			
	Calculated	R_{2tw}	R_{3tw}	A_{2sl}	A_{1sl}	A_{3sl}
*A*120°	Observed	R_{3tw}	A_{3sl}			
	Calculated	R_{1tw}	R_{2tw}	R_{3tw}	A_{2sl}	A_{3sl}
*C*180°	Observed	R_{3tw}	C_{sl1}			
	Calculated	R_{2tw}	R_{3tw}	R_{1tw}	A_{2sl}	C_{sl1}
*C*270°	Observed	R_{2tw}	R_{3tw}	R_{1tw}		
	Calculated	R_{2tw}	R_{3tw}	R_{1tw}	A_{2sl}	C_{sl3}
*R*90°	Observed	R_{2tw}	R_{3tw}	C_{sl3}		
	Calculated	R_{2tw}	R_{3tw}	R_{1tw}	C_{sl3}	A_{3sl}
*R*180°	Observed	R_{2tw}	A_{2sl}			
	Calculated	R_{2tw}	R_{3tw}	A_{1sl}	A_{2sl}	A_{3sl}

based on the plastic deformation parameter calculations, for all six cutting orientations investigated in this study (matching systems are indicated as bold letters). In the table, all the plastic deformation modes observed in the shear strain plots and the 5 most likely plastic deformation systems based on the model are listed. In the C270°, R90°, and R180° cutting orientations, the predicted and observed deformation mechanisms matched to a large extent. For the other cases, certain deformation systems with high plastic deformation parameter values were not observed in the shear strain plots. One possible explanation for this discrepancy is that some plastic deformation systems have orientations that are challenging to identify in our MD simulation setup, which has limited material size in the lateral direction in addition to multiple slip/twinning systems having a similar activation probability. However, it must be noted that the observed deformation mechanisms were among the 5th most likely plastic deformation systems predicted in all the cases.

3.2. *Fracture activation predicted using cleavage fracture parameter*

In the MD simulations conducted for this research, crack formation was observed in five out of the six cutting directions examined (A60°, A120°, C180°, C270°, R90°), Fig. 6. To verify the ability of the slip/fracture activation model to accurately predict fracture activation in MD simulations, calculated results of the cleavage fracture parameters were compared with the fracture observed in OVITO. The crack surfaces were identified by measuring the angle of the cleaved surfaces with the cutting plane.

Subsequently, calculation of the cleavage fracture parameter was performed around the region where the cracks initiated. For the analysis, a target area with a radius of 50 Å, centered on the material point where the crack initiated was defined, and within this designated region, the cleavage fracture parameter was calculated.

Fig. 7 (a) presents the shear strain plot at the time of crack initiation (t_{cut} = 170 ps) and propagation (t_{cut} = 180 ps) for the C270° cutting orientation. A schematic view of the crystal structure is included on the below side of the figure to enhance comprehension. In this cutting orientation, fracture was observed on the C-plane. In Fig. 7 (b), the plot displays the cleavage fracture parameter calculated within the target area at 160 ps, which is 10 ps prior to crack initiation. The plot demonstrates that the cleavage fracture parameter of the C-plane exhibits the highest value compared to other systems at t_{cut} = 160 ps. Consequently, it is evident that the cleavage fracture parameter effectively predicts crack generation for the C270° cutting orientation.

Table 4 provides a summary of the cleavage surfaces identified using the shear strain plots on OVITO and the predicted fracture mechanisms based on the cleavage fracture parameter results (1st and 2nd most likely systems) for all six cutting orientations investigated. The observed and predicted crack generation planes align well for all cases, showing the robustness of the cleavage fracture parameter in accurately predicting crack initiation.

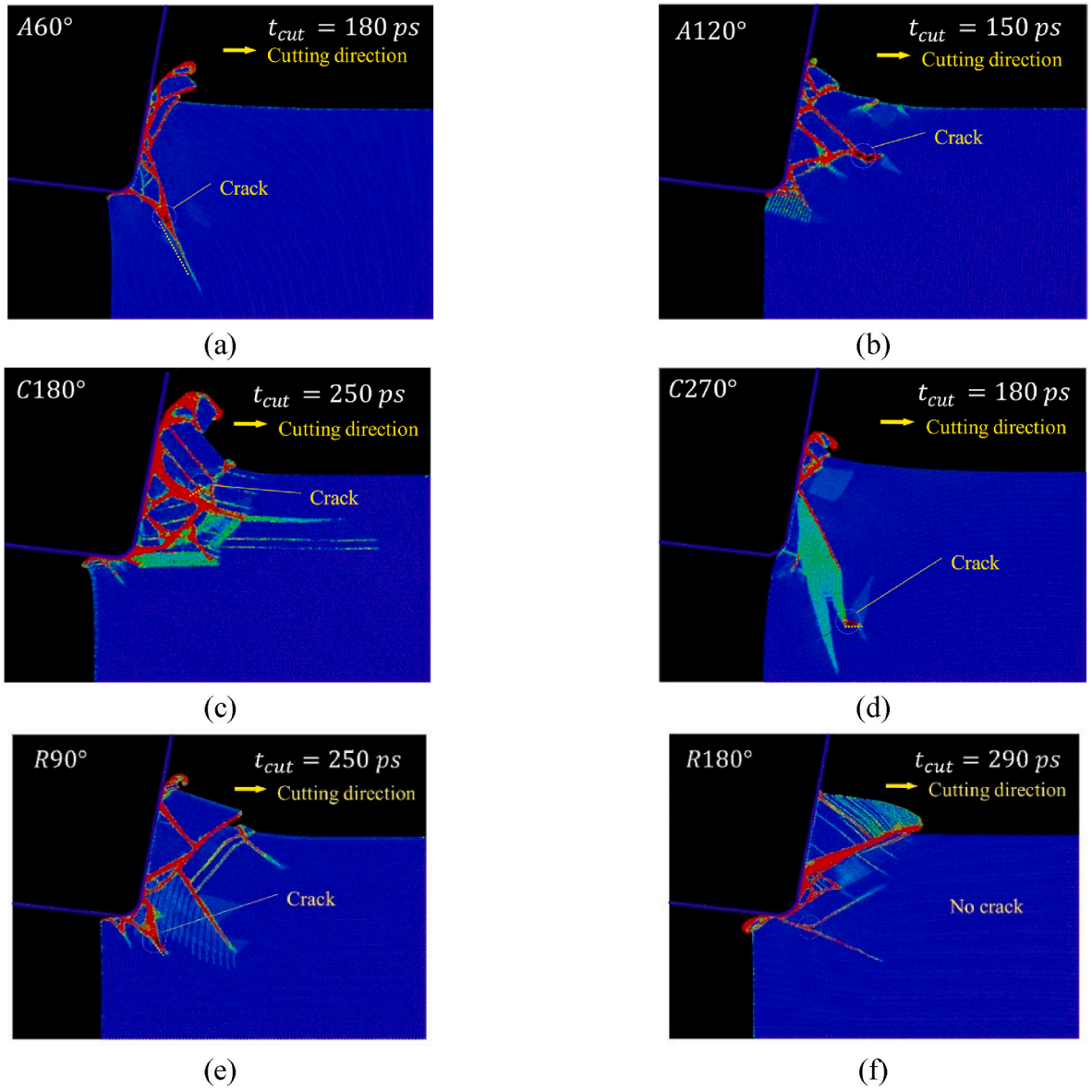

Fig. 6. Crack initiation observed in (a) A60°, (b) A120°, (c) C180°, (d) C270°, (e) R90° cutting orientations, and (f) R180° cutting orientation where no crack was observed.

3.3. Prediction of crack initiation

An equation to predict crack initiation was developed by incorporating both plastic deformation and cleavage fracture parameters. Plastic deformation involves the breaking and formation of atomic bonds between neighboring atoms in a crystalline material as a dislocation/twin boundary moves through the crystal. This process occurs continuously and repeatedly as the deformation progresses. In a scenario such as machining, where the stress field is complex and triaxial, dislocation motion, which temporarily breaks atomic bonds, has the potential to facilitate crack initiation and formation of a new cleaved surface when aligned with a fracture system as shown in Fig. 8.

Based on the proposed idea, the equation to predict crack initiation was formulated as follows:

$$T = C_f F_{max} + C_{pf} P_{F_{max}} F_{max} \tag{3}$$

where T represents the tendency of crack initiation, F_{max} is the maximum cleavage fracture parameter, $P_{F_{max}}$ is the plastic deformation parameter value of the same crystal plane where the maximum cleavage fracture parameter exists and C_f and C_{pf} are fitting coefficients with no units.

For the five cases exhibiting crack initiation, the analysis was conducted using data from 10 ps prior to crack initiation (e.g., if a crack initiation was observed at t_{cut} = 170 ps, the analysis was performed at t_{cut} = 160 ps). This is because once crack initiation commences, it results in void formation, lattice rotation, and stress release, making it challenging to accurately calculate the P and F parameters in the vicinity of the crack. The cleavage fracture and plastic deformation parameters from the target area were obtained and substituted into equation (3). A threshold value of $T = 1$ was assigned to signify crack initiation. A total of five sets (Table 5) of cleavage fracture and plastic deformation values that should satisfy $T = 1$ from the target area of each case were used with the least square regression algorithm to determine the C_f and C_{pf} values. From the regression, C_f and C_{pf} were determined to be 2.42 and 2.36, respectively. The results demonstrate the significant impact of P and F interaction on crack initiation.

Fig. 9 presents the results of temporally plotting the evolution of crack initiation tendency (T-value) using equation (3) to the target area of all six cases. With the exception of A60° cutting orientation shown in

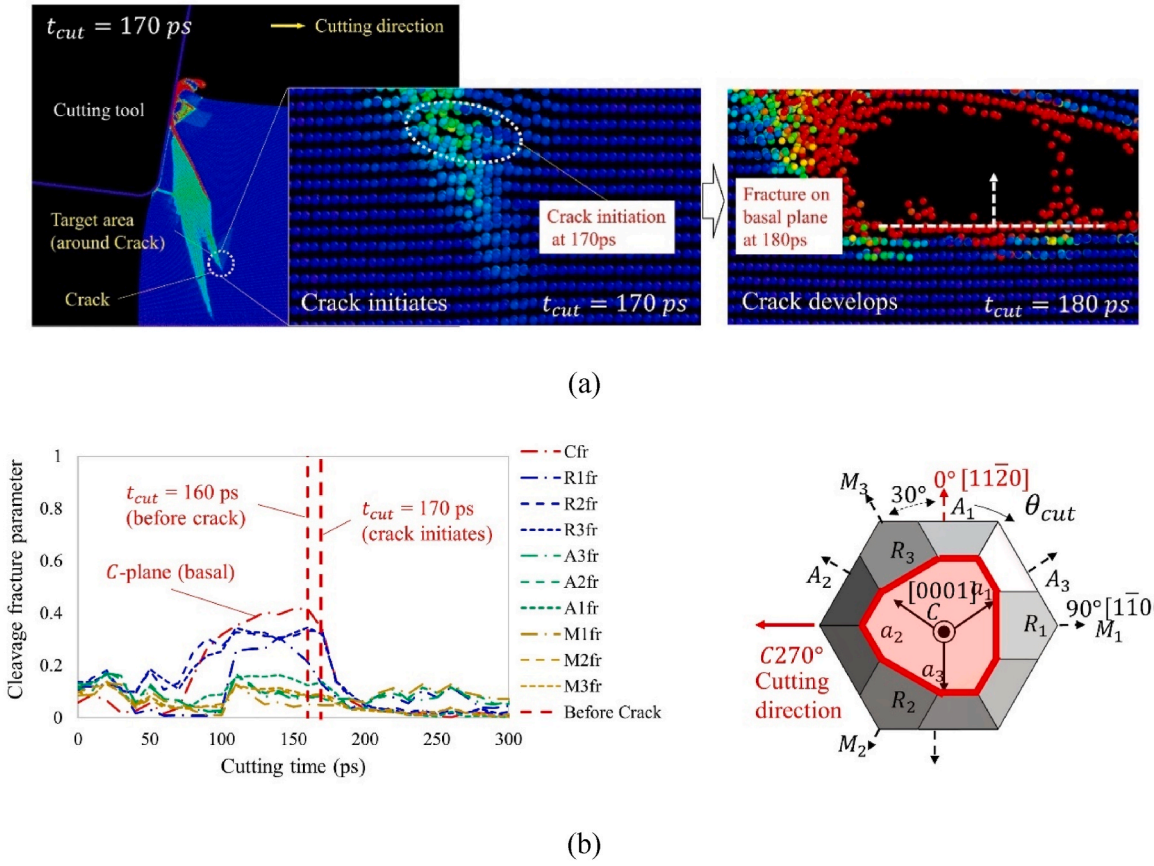

Fig. 7. (a) Crack initiation and development observed by MD simulation and (b) calculated cleavage fracture parameters in the target area for C270° cutting orientation.

Table 4
Summary of observed/predicted fracture systems.

System		1st	2nd
*A*60°	Observed	A_{2fr}	
	Calculated	A_{2fr}	R_{1fr}
*A*120°	Observed	A_{1fr}	
	Calculated	A_{1fr}	M_{2fr}
*C*180°	Observed	R_{3fr}	
	Calculated	R_{3fr}	R_{2fr}
*C*270°	Observed	C_{fr}	
	Calculated	C_{fr}	R_{3fr}
*R*90°	Observed	A_{2fr}	
	Calculated	A_{2fr}	M_{1fr}
*R*180°	Observed	-	-
	Calculated	-	-

Fig. 9 (a), the crack prediction equation for the target area of all cases demonstrated a gradual increase in crack initiation tendency as the cutting time progressed. Moreover, it reached a value of 1 or higher near the observed crack initiation time, thus validating the accuracy of the crack prediction model. Notably, the R180° case depicted in the graph did not exceed a value of 1, which aligned well with the absence of crack initiation in the MD simulation results.

3.4. Comparison between MD simulation and experiment

For the three cases (A60°, C270°, R90°) exhibiting crack formation beneath the tool, the crack morphologies were compared with the experimental results obtained for the corresponding cutting orientations. The cracks were experimentally observed near the region where crack initiation first occurs. However, the cases where cracks initiated in front of the tool in the MD simulations (A120°, C180°) were excluded from this comparison, as it is highly probable that the cracks would be removed by the chip in such scenarios. In those cases, the cracks

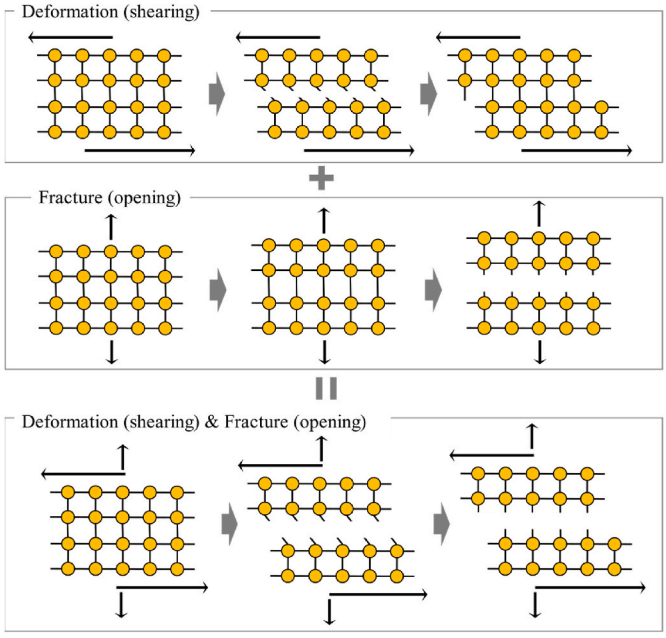

Fig. 8. Influence of interaction between plastic deformation and cleavage fracture to crack generation.

Table 5
Systems of fracture and deformation used for linear regression.

	Time (ps)	Fracture/deformation systems
*A*60°	160	A_{2fr}, A_{2sl}
*A*120°	130	A_{1fr}, A_{1sl}
*C*180°	230	R_{3fr}, R_{3tw}
*C*270°	160	C_{fr} , C_{tw1}
*R*90°	230	A_{2fr}, A_{2sl}
*R*180°	–	-

initiated above the uncut chip thickness. As the MD simulation progressed, these cracks were gradually eliminated through the chip-forming process.

Fig. 10 (a) and (b) show the forces in terms of the cutting time measured in both MD simulations and experiments for the C270° cutting orientation. The cutting time at which crack initiation began was also marked. The force from the MD simulation was obtained by summing all the force components acting on the tool. In the MD simulation, the force exhibits a continuous upward trajectory until the point of crack initiation at 160 ps. Subsequently, it experiences a decline as the crack propagates beyond 160 ps. This phenomenon can be ascribed to the release of stress that had accumulated as the crack opened and advanced. Conversely, in the experimental cutting, the force profile initially presents as relatively smooth when the crack begins to form on the surface. However, as the cutting process progresses, the force undergoes oscillations. This can be explained by the experimental condition, increasing depth of cut. When the depth of cut is small, it results in the formation of smaller surface cracks, which lead to a relatively modest release of stress. This release of stress is insufficient to significantly affect the primary trend of the force. Conversely, when the crack initiates at a greater depth of cut, it undergoes expansion, leading to the release of a more substantial amount of stress. After that, the stress accumulates once more, and as new cracks emerge, this cyclical process repeats, resulting in oscillations in the force measurements [24]. In both cases, it was consistently observed that force is reduced attributed to stress release upon crack initiation.

In the case of A120°, Fig. 11, the cleavage fracture parameter showed

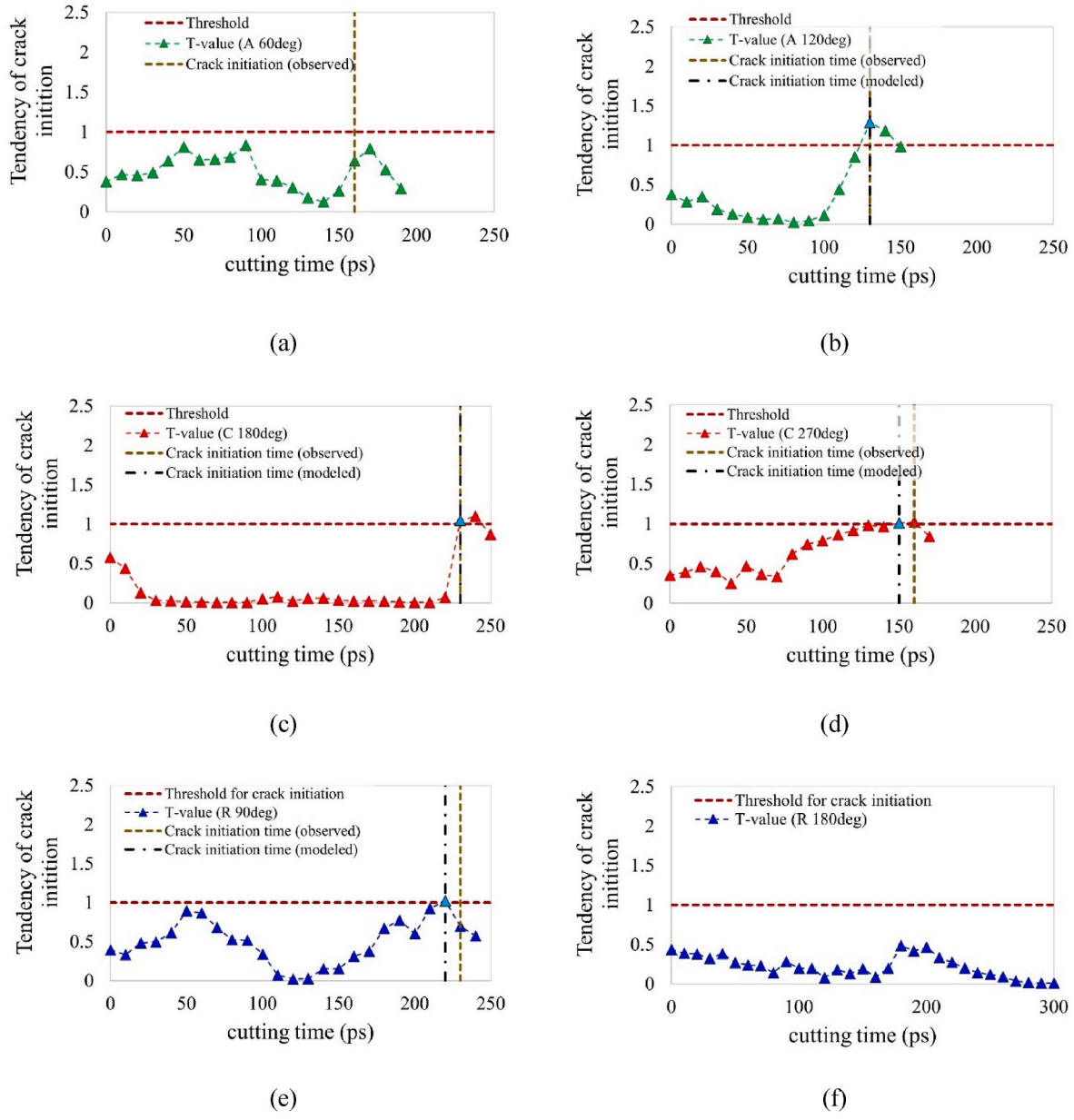

Fig. 9. Tendency of crack initiation for (a) A60°, (b) A120°, (c) C180°, (d) C270°, (e) R90°, and (f) R180° cutting orientations.

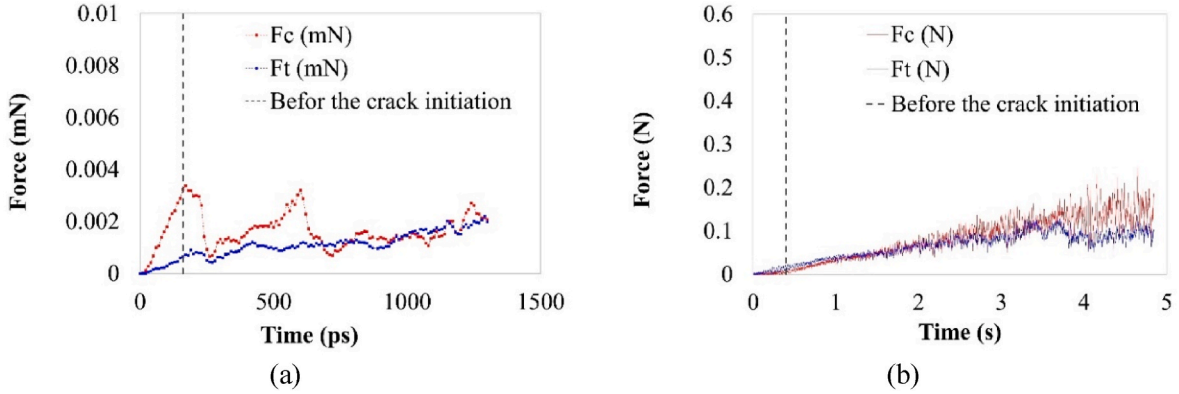

Fig. 10. Force measured by (a) MD simulation and (b) experiment for the C270° cutting orientation.

the highest value for the A_2-plane, but simultaneously, comparable high values were also observed on the R_1-plane. The A_2-plane forms an angle of approximately 60° with the cutting direction A120°, while the R_2-plane is perpendicular to the cutting direction. The crack morphologies observed through SEM in actual experiments exhibited cleavage facets that corresponded to these angles.

The similarity in crack morphology between experiments and MD simulations in the C270° cutting orientation, Fig. 12, has been reported in a previous study [18]. In the C270° case, cleavage fracture exhibited high values specifically on the C-plane, leading to the formation of cracks parallel to the cutting plane and gradually peeling off as the tool progressed, resulting in a layered crack morphology. This observation aligns well with the layered crack morphology found in actual experiments.

In the R90° cutting orientation, Fig. 13, like the case of A120°, the highest cleavage fracture parameter was observed on the A_2-plane. Additionally, high cleavage fracture parameters were observed on the M_1- and R_1-planes. Considering the intersection line between the A_2-plane and the cutting plane R_1, it was anticipated that a diagonal-shaped crack morphology would occur. Furthermore, considering M_{1fr} and R_{1fr} cleavages, a lamellar crack morphology was expected. These predictions aligned well with the crack morphology observed in the experimental results.

4. Conclusion

In this paper, the authors developed a 3-dimensional slip/fracture activation model and used it to calculate plastic deformation and cleavage fracture activation in MD simulations of orthogonal cutting of sapphire. The calculated results matched the observed deformation activations and accurately represented fracture activations, as observed through shear strain plots. In some cases, the plastic deformation parameter value was larger for systems other than the actual observed

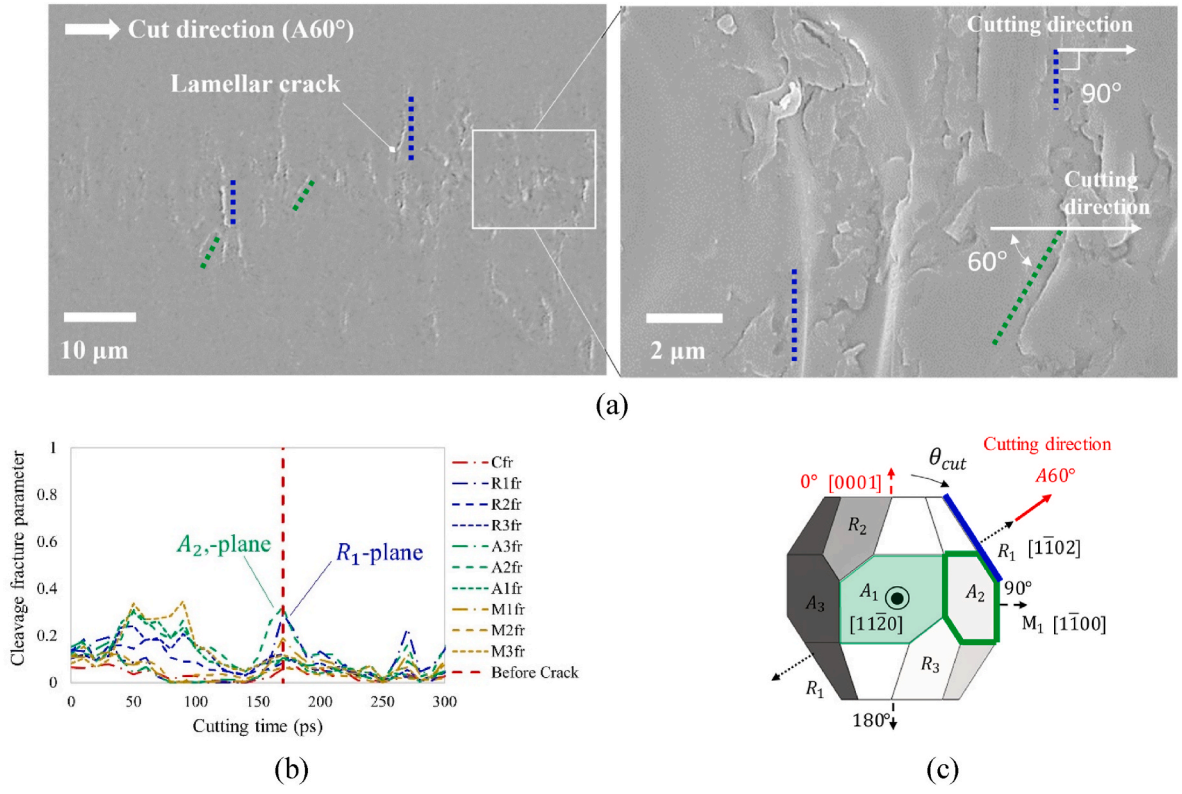

Fig. 11. (a) SEM images depicting crack morphology, (b) calculated cleavage fracture parameter, and (c) schematic view of crystal structure for A60° cutting orientation.

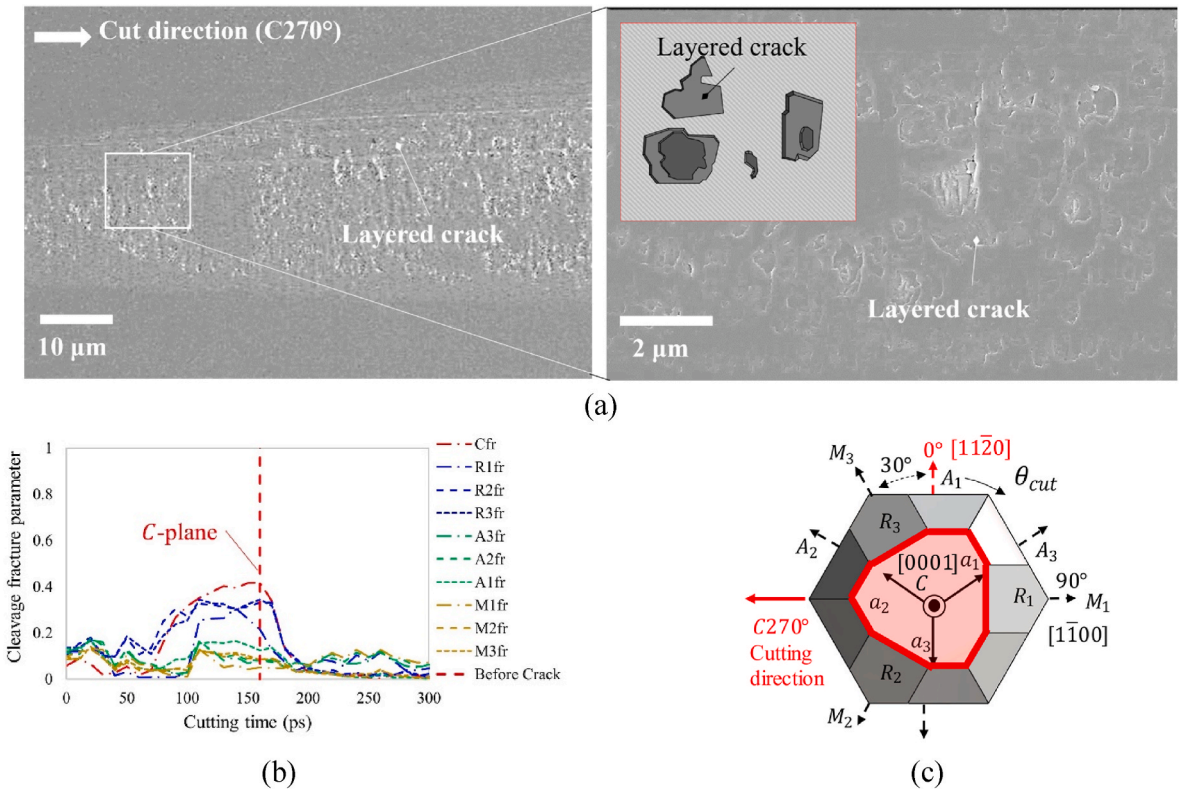

Fig. 12. (a) SEM images depicting crack morphology, (b) calculated cleavage fracture parameter, and (c) schematic view of crystal structure for C270° cutting orientation.

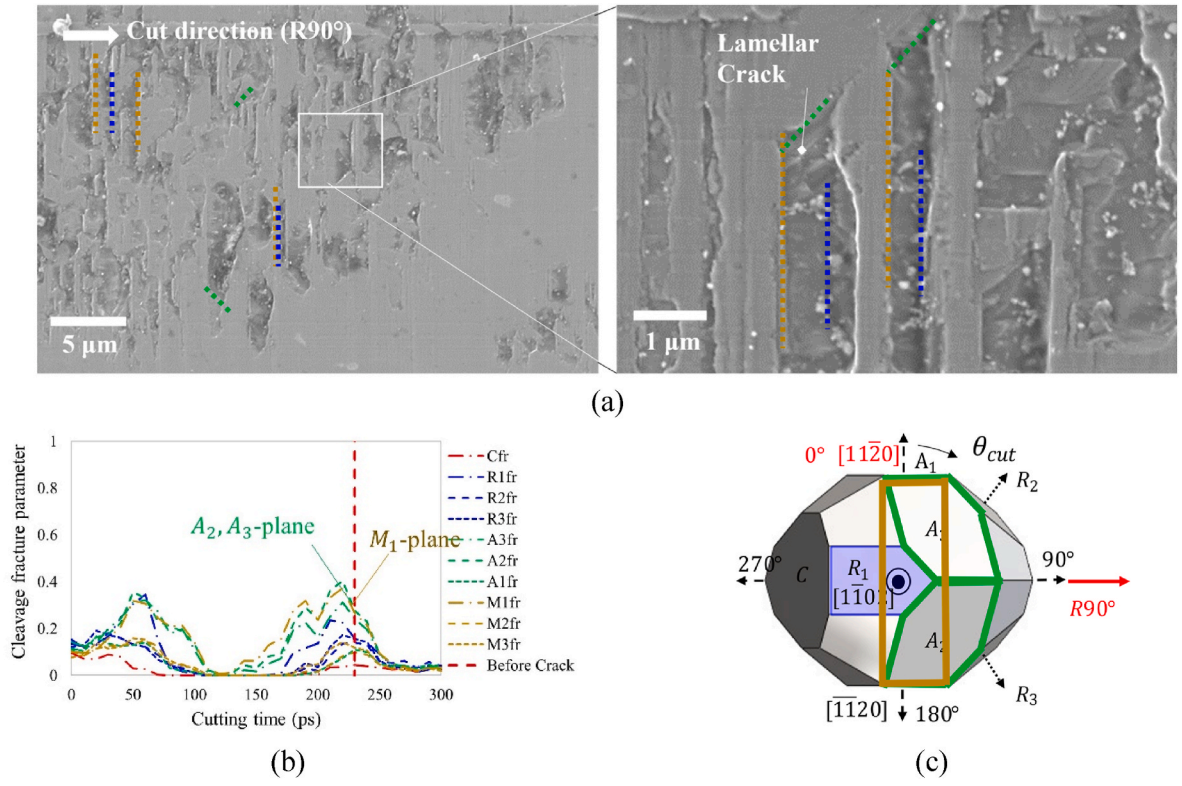

Fig. 13. (a) SEM images depicting crack morphology, (b) calculated cleavage fracture parameter, and (c) schematic view of crystal structure for R90° cutting orientation.

deformation mechanism. This discrepancy may be attributed to the limited width of the MD simulation used in this paper, which may not clearly observe deformation occurring in the lateral direction.

Furthermore, an equation representing the crack initiation tendency was formulated by considering the interaction between plastic deformation and cleavage fracture parameters using linear least square regression. The equation demonstrated that it could reasonably predict crack initiation based on actual MD simulation results. It is necessary to mathematically formulate the interaction between plastic deformations to create a more accurate prediction model. Additionally, it is important to validate the equation by applying it to MD simulation cases with a wider range of conditions.

For a more comprehensive analysis and comparison with experimental results, it is necessary to conduct comparative analyses of MD simulations under various conditions including different depths of cut, cutting speed, and other factors. To analyze and model the interaction between plastic deformations, a more detailed comparison between actual plastic deformations and crack initiation inside the material using transmission electron microscopy (TEM) is required.

Declaration of competing interest

The authors declare that they have no known competing financial interests or personal relationships that could have appeared to influence the work reported in this paper.

Acknowledgements

This material is based on work supported by the National Science Foundation (NSF) under Grant No. CMMI-1844821, No. CMMI-2008563 and No. CMMI-2009150. Authors gratefully acknowledge the kind support from FANUC Corporation, Japan, for the donation of ROBONANO α-0*i*B, ultra-precision machine tool and A.L.M.T. Corporation, Japan, for providing discounted PCD tools to MIN LAB at UW-Madison. The authors gratefully acknowledge use of facilities and instrumentation at the UW-Madison Wisconsin Centers for Nanoscale Technology (wcnt.wisc.edu) partially supported by the NSF through the University of Wisconsin Materials Research Science and Engineering Center (DMR-1720415).

Appendix A. Supplementary data

Supplementary data to this article can be found online at https://doi.org/10.1016/j.precisioneng.2023.12.007.

References

[1] Shen H, Brousseau E, Kulasegaram S. Assessment and validation of SPH modeling for nano-indentation. Comp Part Mech 2023;10:603–13. https://doi.org/10.1007/s40571-022-00514-5.
[2] Matsunaga K, Ii S, Iwamoto C, Yamamoto T, Ikuhara Y. In situ observation of crack propagation in magnesium oxide ceramics. Nanotechnology 2004;15:S376.
[3] Sun S, Peng X, Xiang H, Huang C, Yang B, Gao F, et al. Molecular dynamics simulation in single crystal 3C-SiC under nanoindentation: formation of prismatic loops. Ceram Int 2017;43:16313–8.
[4] Bitzek E, Gumbsch P. Atomistic simulations of dislocation-crack interaction. J Solid Mech Mater Eng 2008;2:1348–59.
[5] Rountree CL, Kalia RK, Lidorikis E, Nakano A, Van Brutzel L, Vashishta P. Atomistic aspects of crack propagation in brittle materials: multimillion atom molecular dynamics simulations. Annu Rev Mater Res 2002;32:377–400. https://doi.org/10.1146/annurev.matsci.32.111201.142017.
[6] Geng Y, Zhang J, Yan Y, Yu B, Geng L, Sun T. Experimental and theoretical investigation of crystallographic orientation dependence of nanoscratching of single crystalline copper. PLoS One 2015;10:e0131886.
[7] Lu C, Gao Y, Deng GY, Michal G, Huynh NN, Liu XH, et al. Atomic-scale anisotropy of nanoscratch behavior of single crystal iron. Wear 2009;267:1961–6.
[8] Pei QX, Lu C, Fang FZ, Wu H. Nanometric cutting of copper: a molecular dynamics study. Comput Mater Sci 2006;37:434–41.
[9] Guo X, Li Q, Liu T, Kang R, Jin Z, Guo D. Advances in molecular dynamics simulation of ultra-precision machining of hard and brittle materials. Front Mech Eng 2017;12:89–98. https://doi.org/10.1007/s11465-017-0412-7.
[10] Kim WK, Kim BH. A molecular dynamics study on atomistic mechanisms of nanoscale cutting process of sapphire. J Mech Sci Technol 2017;31:4353–62. https://doi.org/10.1007/s12206-017-0834-5.
[11] Cai MB, Li XP, Rahman M. Study of the mechanism of nanoscale ductile mode cutting of silicon using molecular dynamics simulation. Int J Mach Tool Manufact 2007;47:75–80. https://doi.org/10.1016/j.ijmachtools.2006.02.016.
[12] Goel S, Kovalchenko A, Stukowski A, Cross G. Influence of microstructure on the cutting behaviour of silicon. Acta Mater 2016;105:464–78.
[13] Lin J, Jiang F, Xu X, Lu J, Tian Z, Wen Q, et al. Molecular dynamics simulation of nanoindentation on c-plane sapphire. Mech Mater 2021;154:103716.
[14] Kim WK, Xi D, Kim BH. Nanoscale indentation and scratching tests of single crystal sapphire using molecular dynamics simulation. Comput Mater Sci 2019;170:109195.
[15] Wunderlich W, Awaji H. Molecular dynamics — simulations of the fracture toughness of sapphire. Mater Des 2001;22:53–9. https://doi.org/10.1016/S0261-3069(00)00044-3.
[16] Kwon SB, Nagaraj A, Xi D, Du Y, Kim DN, Kim WK, et al. Studying crack generation mechanism in single-crystal sapphire during ultra-precision machining by MD simulation-based slip/fracture activation model. Int J Precis Eng Manuf 2023;24:715–27. https://doi.org/10.1007/s12541-023-00776-w.
[17] Dobrovinskaya ER, Lytvynov LA, Pishchik V. Sapphire: material, manufacturing, applications. Springer Science & Business Media; 2009.
[18] Vashishta P, Kalia RK, Nakano A, Rino JP. Interaction potentials for alumina and molecular dynamics simulations of amorphous and liquid alumina. J Appl Phys 2008;103:083504. https://doi.org/10.1063/1.2901171.
[19] Thompson AP, Aktulga HM, Berger R, Bolintineanu DS, Brown WM, Crozier PS, et al. LAMMPS-a flexible simulation tool for particle-based materials modeling at the atomic, meso, and continuum scales. Comput Phys Commun 2022;271:108171.
[20] Kwon SB, Nagaraj A, Yoon H-S, Min S. Study of material removal behavior on R-plane of sapphire during ultra-precision machining based on modified slip-fracture model. Nanotechnol Prec Eng 2020;3:141–55.
[21] Mizumoto Y, Maas P, Kakinuma Y, Min S. Investigation of the cutting mechanisms and the anisotropic ductility of monocrystalline sapphire. CIRP Ann - Manuf Technol 2017;66:89–92. https://doi.org/10.1016/j.cirp.2017.04.018.
[22] Iwasa M, Bradt RC. Fracture toughness of single-crystal alumina. Adv Ceram 1984;10:767.
[23] Stukowski A. Visualization and analysis of atomistic simulation data with OVITO–the Open Visualization Tool. Model Simulat Mater Sci Eng 2009;18:015012.
[24] Bum Kwon S, Min S. Characteristics of force generation on C-, R-, A-and M-planes of single-crystal sapphire during ultra-precision machining. Manuf Lett 2022;33.